ARTICLE

Destructive Quantum Interference in Meta- Oligo (Phenyleneethynylene) Molecular Wires with Gold-Graphene Hetero-junctions

Received 00th January 20xx,
Accepted 00th January 20xx

DOI: 10.1039/x0xx00000x

Yinqi Fan, [a,b] Shuhui Tao,[a,c] Sylvain Pitié,[d] Chenguang Liu,[e] Chun Zhao,[e] Mahamadou Seydou,[f] Yannick J. Dappe,[g] Paul J. Low,[h] Richard J. Nichols [b] and Li Yang*[a,b]

Quantum interference (QI) is well recognised as a significant contributing factor to the magnitude of molecular conductance values in both single-molecule and large area junctions. Numerous structure-property relationship studies have shown that *para*-connected oligo(phenyleneethynylene) (OPE) based molecular wires exemplify the impact of constructive quantum interference (CQI), whilst destructive quantum interference (DQI) effects are responsible for the orders of magnitude lower conductance of analogous *meta*-contacted OPE derivatives, despite the somewhat shorter effective tunnelling distance. Since molecular conductance is related to the value of the transmission function, evaluated at the electrode Fermi energy, $T(E_F)$, which in turn is influenced by the presence and relative energy of (anti)resonances, the relative single-molecule conductance of *para*- and *meta*-contacted OPE-type molecules is influenced both by the anchor group and the nature of the electrode materials used in the construction of molecular junctions (gold|molecule|gold vs gold|molecule|graphene). It is shown here that whilst amine contacted junctions display little influence of the electrode material on molecular conductance, due to the similar electrode-molecule coupling through this anchor group to both types of electrodes, the weaker coupling between thiomethyl and ethynyl anchors and the graphene substrate electrode results in a relative enhancement of the DQI effect. This work highlights an additional parameter space through which to explore QI effects and establishes a new working model based on the electrode materials and anchor groups in tuning QI effects beyond the chemical structure of the molecular backbone.

Introduction

Both experimental and theoretical studies of single molecular junctions (SMJs) have greatly contributed to the understanding of charge transport through single molecular wires and bridges and this has given great impetus to the field of molecular electronics. [1-5] Over the last decade these studies have allowed direct elucidation of coherent transport phenomena in charge transport through molecules, and the identification of quantum interference (QI) effects. [6-9] The various features arising from QI can be broadly classified as either constructive quantum interference (CQI) and destructive quantum interference (DQI) effects. CQI was observed in molecular junctions (MJs) with linearly conjugated backbones, such as *para*-connected phenylene rings[10], including examples where two such systems are connected in parallel.[11] In contrast, DQI occurs in molecular systems containing electron transport channels that result in the emergent de Broglie waves arriving at the drain electrode with phase differences; prominent examples arise in molecular backbones based on *meta*-substituted phenylene rings [12, 13], and cross-conjugated systems. [14, 15] The experimentally determined conductance of SMJs impacted by DQI can be several orders of magnitude smaller than that of SMJs without DQI.[12,13, 16,17]

DQI can often be recognised by a characteristic sharp dip in the plot of the theoretically computed transmission function, $T(E)$, against the electron energy, E.[13, 18] As the position of this DQI-induced dip in the transmission function relative to the electrode Fermi level, E_F, can be tuned through heteroatom substitution in the backbone [19, 20] or via selectively positioned substituents,[21, 22] it is possible to use DQI features as a further degree of chemical-design induced control over the electrical properties of a SMJ. In addition, electrochemical gating can be used to control the energetic position of the DQI feature, since the characteristic dip in electronic transmission can be shifted in energy, which facilitates tuning of the molecular junction conductance. This has enabled electrochemically-modulated control of the junction conductance by two orders of magnitudes.[23-25] It has also been reported that molecular layers

[a.] *Department of Chemistry, Xi'an-Jiaotong Liverpool University, Suzhou, 215123, China.*
[b.] *Department of Chemistry, University of Liverpool, Liverpool, L69 7ZD, UK.*
[c.] *NUS (Chongqing) Research Institute, Chongqing, China*
[d.] *Applied Quantum Chemistry group, E4, IC2MP, UMR 7285 Poitiers University CNRS, 86073 Poitiers, France*
[e.] *Department of Electrical and Electronic Engineering, Xi'an-Jiaotong Liverpool University, Suzhou, 215123, China.*
[f.] *Université de Paris, ITODYS, CNRS, Paris F-75006, France*
[g.] *SPEC, CEA, CNRS, Université Paris-Saclay, CEA Saclay 91191 Gif-sur-Yvette Cedex, France.*
[h.] *School of Molecular Sciences, University of Western Australia, 35 Stirling Highway, 6009 Crawley, Australia† Footnotes relating to the title and/or authors should appear here.*
Electronic Supplementary Information (ESI) available: [details of any supplementary information available should be included here]. See DOI: 10.1039/x0xx00000x

showing DQI exhibit significant rectification under electrochemical control.[26] Peng et al. have shown that the magnitude of the effect of DQI on the single-molecule junction conductance is sensitive to the composition of the (metal) electrodes.[27] Similarly, the alignment of the DQI dip with respect to the electrode Fermi level is sensitive to the nature of the anchor groups contacting the molecule within the junction to the electrode; however, these changes in electrode composition or anchor group do not disturb the fundamental property of DQI induced by the backbone structure.[28]

Beyond tuning the electrical conductance, the impact of DQI in SMJs on other materials properties has also been demonstrated. For example, the thermopower of a molecular junction is related to the first derivative of the transmission function evaluated at the Fermi level (E_F) *i.e.* $S(E_F) \approx -S_0(dlnT(E)/dE)_{E=E_F}$, where E is in eV and $S_0 = \alpha T$ (α is the Lorentz number, T is temperature in K). Therefore, molecular junctions showing DQI can exhibit significantly enhanced thermopower when compared with molecular junctions without the sharply sloped features in $T(E)$ induced by the DQI feature.[29] These combined results show the potential of molecular targets exhibiting DQI to be used in a variety of scenarios to modulate the electrical and materials properties of molecular-based molecular devices. [30-33]

Although many 'large area' molecular junctions are often constructed with different materials comprising the substrate and top electrodes by experimental necessity,[34] the majority of studies of the electrical characteristics of SMJs have used "symmetric" anchoring of the molecular target in the junction. In other words, the molecule within the junction has been contacted to the left and right electrodes of the same type, E_L and E_R, via the same anchoring group, X, at each terminus (*e.g.* E_L|X-backbone-X|E_R). By contrast, the electrical properties of "asymmetric" SMJs, where the left and right contacts are differentiated by the nature of the electrode materials or contacting groups, are less commonly examined. However, there is an emerging body of evidence that highlights the opportunities that asymmetric SMJs offer for exploring and optimising electrical effects. For example, indium tin oxide (ITO)|molecule|gold SMJs present an excellent selectivity and control over molecular orientation when forming molecular junctions with "asymmetric" anchoring groups (different groups at either end of the molecule).[35] Beyond wire-like conductance, graphite|molecule|Au junctions featuring α,ω-diamino oligo(phenylene)s exhibit rectifying properties due to asymmetric coupling to the two electrodes,[36] whilst gold|molecule|graphene hetero-junctions induce a reduction of the attenuation factors (β) of symmetrically functionalised alkanes and oligo(phenylene ethynylene)-based SMJs. [37, 38]

In this work the electrical properties of *para*- and *meta*-connected oligo(phenylene ethynylene) (OPE) molecules contacted within symmetric (gold|molecule|gold) SMJs and asymmetric gold|molecule|graphene single molecule hetero-junctions by one of three different anchoring groups (amine, methyl sulfide and ethynyl) have been determined. Whilst as noted above, the anchoring group and electrode type has been used to tune the relative energies of the electrode Fermi level and the DQI induced dip in $T(E)$ in symmetric SMJs, here comparison of the respective single molecule conductances from gold|molecule|gold and gold|molecule|graphene SMJs allow exploration of these effects in asymmetric junctions. It has been previously reported that amine and methyl sulfide groups are connected with gold electrodes through dative bonds, while they connect with graphene by van der Waals forces.[39-43] The interest in an ethynyl anchoring group lies in the spontaneous formation of a covalent bond with gold and concomitant loss of a hydrogen atom.[44, 45] The use of ethynyl contacts has resulted in SMJs displaying higher conductance than the equivalent molecules anchored through thiol chemisorption chemistry, and as such this provides additional interest in extending the use of this anchor group here.[46] To the best of our knowledge, this is the first report of hetero-junctions influenced by destructive quantum interference. The theoretical study shows that the different couplings between electrodes and anchoring groups make the dip of transmission spectrum shift and results in conductance changes of the molecules studied.

Experimental and computational section

Compounds

The compounds 1,4-bis(4-aminophenylethynyl) benzene (PN), 1,4-bis(4-thiomethylphenylethynyl) benzene (PS), 1,4-bis(4-ethynylphenylethynyl) benzene (PC), 1,3-bis(4-aminophenylethynyl) benzene (MN), 1,3-bis(4-thiomethylphenylethynyl) benzene (MS), and 1,3-bis(4-ethynylphenylethynyl) benzene (PC) (Figure 1) were prepared by literature methods,[47-50] or minor variations, and characterised as detailed in the SI.

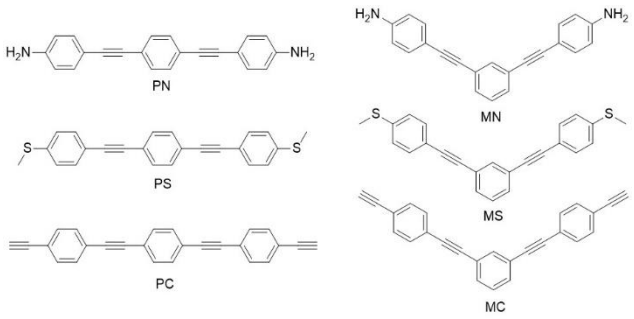

Figure 1 The *para* and *meta*-connected analyte molecules used in this work

Single-molecule conductance

Molecular conductance measurements were made using the STM-*I(s)* technique.[51] The STM tip, which is used as the top contact, was fabricated from a gold wire (Tianjin Lucheng Metal) with a diameter of 0.25 mm and purity of 99.99%, using an electrochemical etching method.[52] The 1×1 cm gold on borosilicate glass and graphene on nickel substrates were purchased from Arrandee® (Germany) and The Graphene Supermarket (USA), respectively. All conductance measurements were performed in mesitylene (Sigma Aldrich, 99%) solutions containing 0.1 mM of the target molecule. In the

measurement process, the gold tip was held above the substrate at an initial vertical distance (4 nm) and then gradually approached to the substrate until the tunneling current reached the set point current. After that, the tip was retracted to zero tunneling current and further retracted for 4 nm to ensure that the tip was sufficiently retracted from the substrate. During this process, the molecular target could be captured between the electrode pair thereby forming a single molecule junction (SMJ). The set point current is adjusted to control the distance between the tip and the substrate, ensuring that there is no direct contact between the upper and lower electrodes during the extension and retraction cycles. The tip bias was set to +0.3 V for all the measurements. Over 10000 current-distance *I*-(*s*) curves were collected for each analysis. The *I*-(*s*) curves with conductance plateaus were collected through a fully automatic sorting program developed locally and plotted as 1D conductance histograms.[53] The most probable single molecule conductance of each molecule was obtained from Gaussian fitting to the prominent feature in these histograms.

Computational methods

In order to support the experimental measurements, Density Functional Theory (DFT) calculations have been performed using the Fireball code,[54] following the same procedure as detailed elsewhere for oligophenylene ethynylene-based molecular junctions.[38] This approach is based on a self-consistent version of the Harris–Foulkes LDA functional,[55] instead of the traditional Kohn–Sham functional. The potential is calculated by approximating the total charge by a superposition of spherical charges around each atom. The Fireball simulation package also uses a localized optimized minimal basis set,[56] and the self-consistency is achieved over the occupation numbers through the Harris functional.[57] Besides, the LDA exchange–correlation energy is calculated using the efficient multi-center weighted exchange–correlation density approximation (McWEDA). [58, 59] The cut-off radii (in atomic units) of the optimised numerical orbitals (sp^3d^5) used for the present calculations are *s* = 4.6, *p* = 5.2, *d* = 4.2 (gold), *s* = 4.1, *p* = 4.5 (C), *s* = 4.2, *p* = 4.2 (N), *s* = 3.1, *p* = 3.9 (S), and *s* = 4.1 (H). This basis set has been used to determine the structural and electronic properties of the molecular junctions.[20, 60] For the molecular junctions, we considered the *meta*-structured molecules presented in Figure 1, sandwiched between gold electrodes or gold and graphene electrodes. In these simulations, the gold electrodes are represented by pyramids of 35 atoms, and the graphene substrate by a 5 × 5 graphene supercell in the XY plane. Structural properties have been determined by optimising the corresponding geometry until the forces fell below 0.1 eV/Å. Finally, we determine the electronic transmission and conductance by using a non-equilibrium Green function (NEGF) formalism within a fast Fisher-Lee approach.[61] As it is well-known, the determination of the Fermi level is of crucial importance for electronic transport calculations in molecular junctions. Here it is even more important in the case of *meta* junctions, since the position of the DQI dip with respect to the Fermi level changes the value of the calculated conductance dramatically. Here the Fermi level is determined as the minimum of the Density of States (DOS) between the HOMO and LUMO levels.[61] This determination is obviously not perfect, but has been found to give results in rather good agreement with the experiment.[61]

Results and discussions

The compounds PN, PC, PS, MN, MC, and MS each feature one of two distinct backbone geometries with linearly conjugated (*para*-OPE) or non-linear meta-connected (*meta*-OPE) π-electronic structures and one of three functional groups of varying inductive electron donating and withdrawing properties that can serve as electrode contacting groups. The solid UV-vis spectra of studied molecules were measured using the UV-vis Spectrophotometer (Agilent, Cary 300 UV-VIS analyser) with an integrating sphere (Agilent, DRA-CA-30I). In dichloromethane solution, the absorption spectra of members of the *para*- (P) (Figure 2a) and *meta*- (M) (Figure 2b) series are similar with the low energy absorption edge of the *para* series exhibiting greater sensitivity to the electronic character of the substituents. However, to eliminate solvation effects, and thus better estimate the HOMO-LUMO gap, the spectra were also recorded in the solid state and analysed through the Tauc method, commonly used to determine the optical band gap in organic semiconductors. [62] The relationship between optical band gap and absorption coefficient (α) follows the equation: $(\alpha h\nu)^2 = B(h\nu - E_g)$, where *h* is Planck's constant, *ν* is the frequency of the incident photons, *B* is a constant and E_g is the band gap;[63] for organic semiconductors, E_g can be approximated as a HOMO-LUMO gap.[64-66]

As shown in Figure 2d, the band gaps of the target molecules are determined as the intersection of the respective tangents derived for each peak with the horizontal coordinate. The resulting estimates gave similar HOMO-LUMO gaps for molecules within each family (PN (2.7 eV), PS (2.8 eV), PC (2.8 eV); and MN (3.1 eV), MS (3.2 eV), MC (3.2 eV)), with the *meta*-connected OPEs giving larger HOMO-LUMO gaps than the linearly *para*-connected compounds as might be reasonably expected.[67, 68] These data further demonstrate that the electronic structures of each member of a series are similar, and little perturbed by the anchor groups. Consequently, any differences in the electronic behaviour of members of a series within a molecular junction likely arise from the nature of the molecule-electrode contact and associated molecule-electrode coupling.

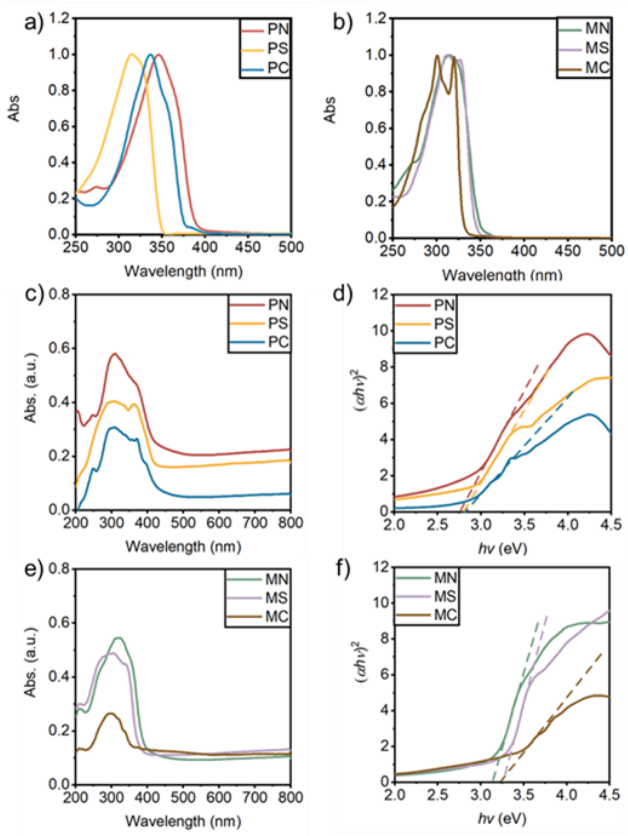

Figure 2 a) and b) Normalised absorption spectra of target molecules; c) and e) Solid UV-vis spectra and d) and f) Tauc plots of target molecules

To explore the various and combined effects of electrode materials and anchor groups on the electrical characteristics of these molecules, the single-molecule conductance of each member of both series was determined within single-molecule gold|molecule|gold homo-junctions and gold|molecule|graphene hetero-junctions using the *I*(*s*) technique. [69] The resulting 1D conductance histograms together with representative *G*-*s* traces are given in Figures 3 – 5 and summarised in Table 1. In each case, the most probable molecular conductance was determined by fitting the Gaussian distribution (black lines) to the peak in the conductance histogram. The error bar of each most probable molecular conductance was calculated from the half-peak width of the conductance peak. The most probable molecular conductance value of PN in a gold-gold junction was measured to be 13 ± 1.8 nS, in good agreement with the values reported by Ferradás *et al.* [70] and Lu *et al.* [71] An essentially identical value (13 ± 2.8 nS) was also determined for the molecular conductance of PN in a gold|molecule|graphene junction (Figure 3, Table 1). The molecular conductance of the analogous *meta*-OPE MN is approximately an order of magnitude lower in both

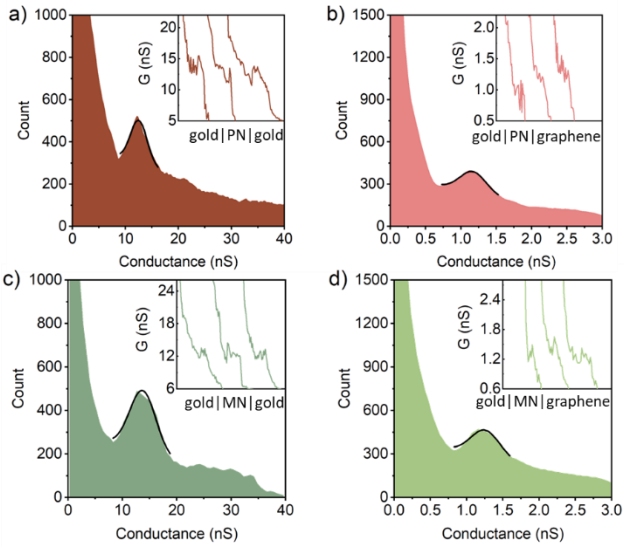

Figure 3 1D conductance histogram of PN in a) gold|molecule|gold junctions and b) gold|molecule|graphene junctions, and MN in c) gold|molecule|gold junctions and d) gold|molecule|graphene junctions. The black lines represent the Gaussian peak fitting to the most prominent feature in these histograms. The insets represent the representative *I*(*s*) curves of studied molecular junctions.

gold|molecule|gold (1.1 ± 0.21 nS) and gold|molecule|graphene (1.1 ± 0.23 nS) junctions due to the pronounced DQI dip near the electrode Fermi level in the transmission functions of *meta*-phenylene structures.[72] It is apparent that the changes in electrode material have little to no measurable effect on the most probable molecular conductance of these amine contacted compounds.

In a similar manner, the 1D conductance histograms of the thioether anchored *para-OPE* contain conductance peaks corresponding to an essentially identical most probable conductance in gold-gold (8.2 ± 1.6 nS) and gold-graphene (8.2 ± 1.5 nS) single-molecule junctions. As expected, the molecular conductance of the *meta*-connected analogue, MS, in gold|molecule|gold and gold|molecule|graphene junctions are substantially lower, being 0.56 ± 0.09 nS and 0.39 ± 0.10 nS, respectively (Figure 4, Table 1).

ARTICLE

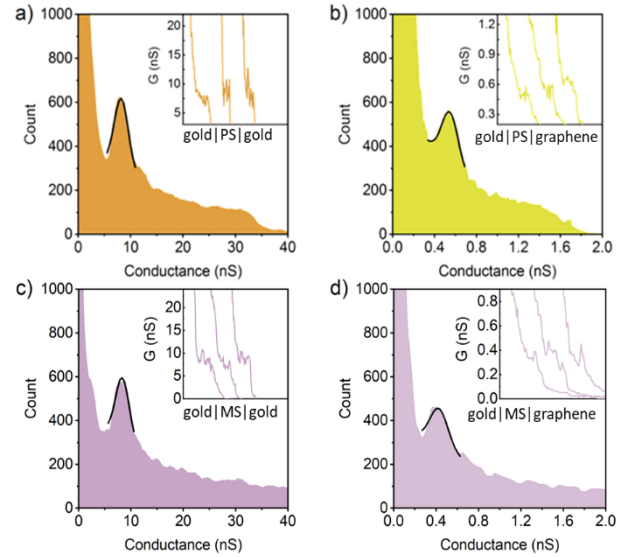

Figure 4 1D conductance histogram of PS in a) gold|molecule|gold junctions and b) gold|molecule|graphene junctions, and MS in c) gold|molecule|gold junctions and d) gold|molecule|graphene junctions. The black lines represent the Gaussian peak fitting to the most prominent feature in these histograms. The insets represent the typical *I*(*s*) curves of studied molecular junctions

In single-molecule gold|molecule|gold junctions, the conductance of the ethynyl-contacted PC is found to be around 19 ± 3.7 nS, which is higher than both the amine (PN) and thiomethyl (PS) contacted analogues, but comparable with other ethynyl-contacted three-ring OPEs,[73] reflecting the stronger molecule-electrode electronic coupling (Figure 5, Table 1). This difference in coupling arises from the fact that, in contrast to the amine and thioether anchors which bind to both gold and graphene through a combination of dative and electrostatic interactions and van der Waals forces, the terminal alkyne undergoes a dehydrogenation reaction at gold surfaces, to create a strong covalent gold|-C≡C interaction.[45, 74-76] Comparing the interactions of the studied molecules with gold electrodes, the stronger interaction between gold and ethynyl lead to gold|PC|gold junction exhibiting higher conductance values than the gold|PN|gold junction and the gold|PS|gold junction. In the gold|PC|graphene hetero-junctions, the ethynyl anchor contacts through as gold|-C≡C, with a direct Au-C bond to the deprotonated acetylene, [44, 45] and a much weaker van der Waals force through C≡C-H|graphene at the graphene electrode. This weaker contact between ethynyl and graphene is associated with a decrease in electrode|molecule coupling. The resulting shift in the alignment of the position of electrode Fermi levels decreases the most probable molecular conductance of PC by a factor of approximately two (9.4 ± 1.3 nS, Figure 5, Table 1).

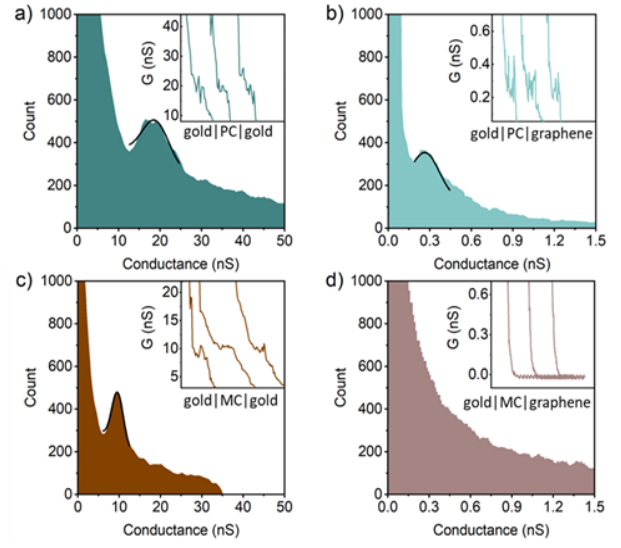

Figure 5 1D conductance histogram of PC in a) gold|molecule|gold junctions and b) gold|molecule|graphene junctions, and MC in c) gold|molecule|gold junctions and d) gold|molecule|graphene junctions. The black lines represent the Gaussian peak fitting to the most prominent feature in these histograms. The insets represent the typical *I*(*s*) curves of studied molecular junctions.

Rather strikingly, despite the strong coupling induced by the ethynyl gold|-C≡C contacts, the most probable single-molecule conductance of MC in the gold|molecule|gold junction was found to be 0.27 ± 0.11 nS, which is the lowest of all of the *meta*-connected compounds in these homo-junctions (Figure 5, Table 1). In the gold-graphene hetero-junction, the single-molecule conductance of MC lies below the limits of detection of the instrument used in this study (ca. 10 pA/sample bias, or 0.03 nS). To facilitate the discussion that follows, an upper estimate of the single-molecule conductance value is taken as 0.03 nS; true values may be far lower.

Table 1 Summary of the conductance and conductance ratios of studied MJs

Molecule	Conductance(nS)		Conductance ratio	
	gold-gold	gold-graphene	gold-gold	gold-graphene
PN	13 ± 1.8	13 ± 2.8	12	12
MN	1.1 ± 0.21	1.1 ± 0.23		
PS	8.2 ± 1.6	8.2 ± 1.5	15	21
MS	0.56 ± 0.09	0.39 ± 0.10		
PC	19 ± 3.7	9.4 ± 1.3	70	400*
MC	0.27 ± 0.11	0.03*		

* A value at the noise floor has been assumed here as no current histogram peak was observed. The junction may not form or the single-molecule conductance was below the current sensitivity limit of the equipment.

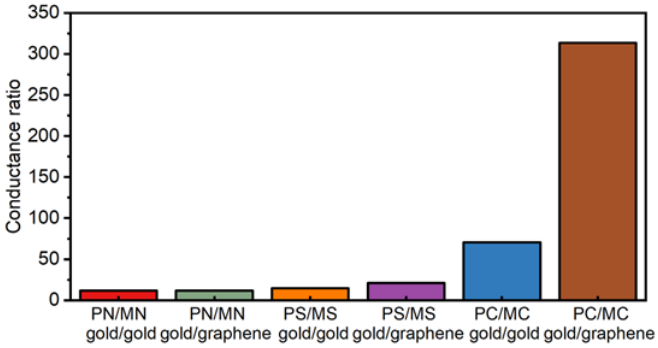

Figure 7 A graphical representation of the conductance ratios of SMJs.

The anticipated effects of the chemical structure of the molecular backbones on molecular conductance regardless of the electrode materials used in the construction of the junction are clear (Table 1). Thus, whilst the linearly conjugated *para*-series (PN [38, 70, 71], PS [38], PC [73]) display CQI and relatively high single-molecule conductance, the emergence of DQI features in the transmission functions at the Fermi levels results in a 1 – 2 order of magnitude decrease in single-molecule conductance of the *meta*- structured analogues (MN, MS, MC). [13, 20, 77] For any given pair of electrodes, changes in the anchor group result in a small variation in the most probable conductance. This observation demonstrates both the robustness of the QI features imposed by the chemical structure of the molecular backbone,[28] and the influence of small changes in the electrode-molecule coupling on the molecular conductance. The relative effects of electrode-molecule coupling, quantum interference and Fermi energy alignment with the (anti) resonance features of the transmission functions that describe charge transport through the junction are collectively expressed within the conductance ratios summarised numerically in Table 1 and graphically in Figure 6. The increasing single-molecule conductance PS < PN < PC observed in the gold|molecule|gold homo-junctions illustrates the role played by electrode-molecule coupling in tuning molecular conductance.[78] A different trend in the magnitude of single molecule conductance values is found for the *meta*-series in gold|molecule|gold single-molecule junctions (MC < MS < MN), clearly indicating the dominant effect of the position of the DQI

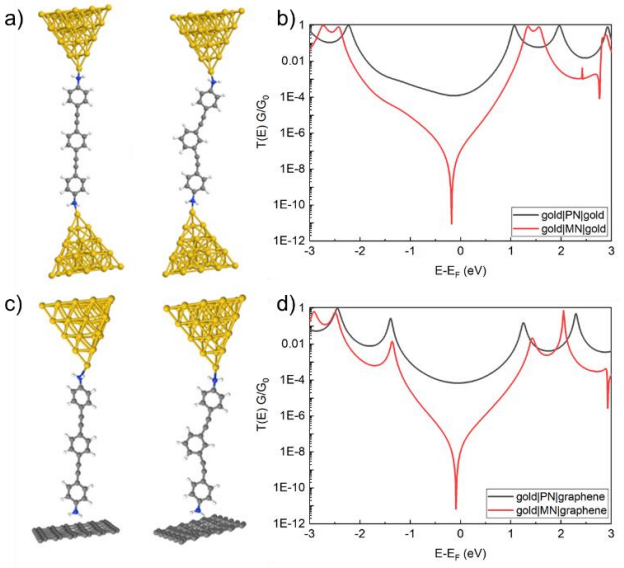

Figure 6 Structural models for PN and MN in a) gold|molecule|gold, and c) gold|molecule|graphene single moelcule junctions, with plots of the corresponding calculated electronic transmission functions plotted in b) and d) (with the black curve for PN, and the red curve for MN; the latter exhibiting the characteristic DQI dip near the Fermi level).

induced dip in the transmission function relative to the electrode Fermi levels on the electronic characteristics of the junction.[79]

In the gold|molecule|graphene hetero-junctions, the variation in conductance is somewhat less distinct with the anchor group due to the common electrostatic interaction of the anchor groups to the graphene electrode. The data indicate that it is only the carbon contacted compounds PC and MC that show any significant decrease in conductance in the hetero-junctions. The single-molecule conductance values of the *meta* series are low, and more sensitive to the anchor group, spanning some two orders of magnitude (1.1 – 0.03 ns). As with the *para*-structure compounds, variations in the electrode-molecule coupling undoubtedly must play some role in this observation, but the greater magnitude of variation points to a key role in the position of the DQI feature relative to the electrode Fermi levels

To gain further insight into these various factors on the electrical conductance of the SMJs investigated here, model junctions were constructed and explored using DFT-based calculations (Figure 7-9, Table 2). Taking the amine-contacted compounds PN and MN within the gold-gold homo-junctions as a point of reference, the calculated transmission curves demonstrate the expected features. The transmission functions for PN features well-separated HOMO and LUMO resonances, which are further separated in the comparable plot for MN, consistent with the greater HOMO-LUMO gap obtained from the optical measurements. As a result of CQI, between the HOMO and LUMO resonances of PN the transmission function describes a broad, relatively flat and rather high conductance region. In contrast, the transmission function for MC features a strong, sharp dip near the calculated Fermi energy. As is now well-appreciated in the literature, [13, 18] this dip explains the

strong difference in magnitude between the conductance in the PN and in the MN configurations.

Moving to the gold|molecule|graphene hetero-junctions formed from PN and MN, remarkably similar transmission curves are obtained, a consequence of the similar mechanism of electrode-molecule coupling through the amine group to both gold and graphene.[38] These results are therefore consistent with the experimentally observed single-molecule conductances (Table 1).

For the thioether contacted compounds PS and MS, we observe a greater shift of the molecular levels between

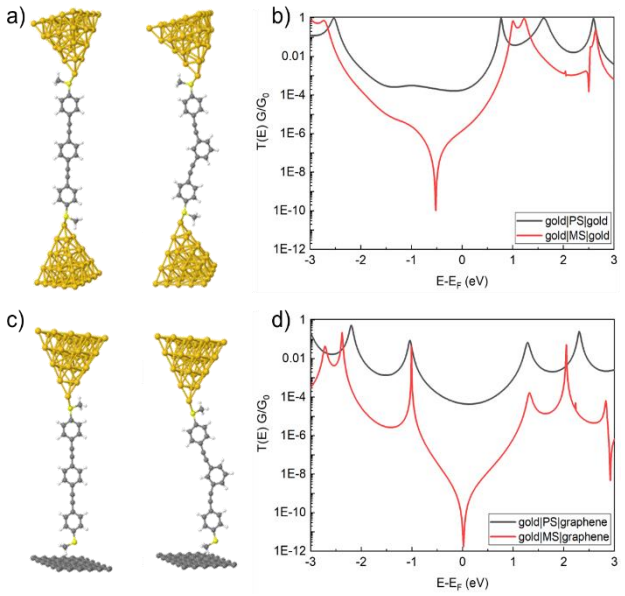

Figure 8 Structural models for PS and MS in a) gold|molecule|gold, and c) gold|molecule|graphene single moelcule junctions, with plots of the corresponding calculated electronic transmission functions plotted in b) and d) (with the black curve for PS, and the red curve for MS; the latter exhibiting the characteristic DQI dip near the Fermi level).

gold|molecule|gold and gold|molecule|graphene junctions, which can be attributed to a difference in electrostatic dipoles as observed in an earlier work (Figure 8).[80] Consequently, the DQI dip lies below the Fermi level for the gold|molecule|gold configuration, whereas it is centred at the Fermi level for gold|molecule|graphene configuration, leading to a very small conductance value for MC in the hetero-junction. However, as in the calculations the dip corresponds to a mathematical singularity, the value obtained is not well suited for comparison to the experimental results.

To the best of our knowledge, no theoretical study of alkyne adsorption on graphene has yet been performed. The adsorption energy of the molecules PC and MC on graphene as a function of the molecule-graphene distance was first explored to estimate the stability of the resulting junctions (Figure S5). The adsorption energy varies as a function of the position of the terminal hydrogen, but the equilibrium position lies around 2-2.5 Å, with an energy of 0.12-0.17 eV/molecule. Consequently, we can assume that this configuration, which has some analogy to the T-shape configuration of a benzene dimer,[81] is stable and allows the formation of a molecular junction.

The results from electronic transmission calculations with PC and MC in gold|molecule|gold and gold|molecule|graphene junctions are shown in Figure 9. For PC, there is a small shift of the electronic transmission function in response to the change in electrode material, which is consistent with the experimental observation. However, for MC, there is a far more significant shift of the position of the DQI dip leading to the substantial difference in the single-molecule conductance values of MC in the homo- and hetero-junctions.

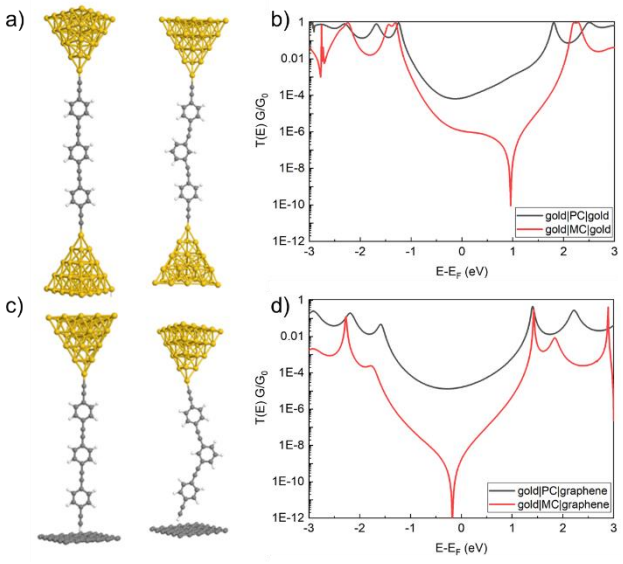

Figure 9 Structural models for PC and MC in a) gold|molecule|gold, and c) gold|molecule|graphene single molecule junctions, with plots of the corresponding calculated electronic transmission functions shown in b) and d) (with the black curve for PC, and the red curve for MC; the latter exhibiting the characteristic DQI dip near the Fermi level).

Table 2 Summary of the calculated single-molecule conductance of PN, PS, PC, MN, MS and MC in gold|molecule|gold and gold|molecule|graphene junctions.

Molecule	Conductance (nS)		Conductance ratio	
	gold-gold	gold-graphene	gold-gold	gold-graphene
PN	10.46	7.53	1162	7530
MN	0.009	0.001		
PS	16.03	3.9	133	260000
MS	0.12	0.000015		
PC	5.57	1.27	51	8466
MC	0.11	0.00015		

From these calculations, several general trends can be illustrated. At the minimised energy configurations the molecule is somewhat "stretched" in the junction. One can observe a correlation between how stretched the molecule is in the *meta* configuration and the position of the DQI dip. Indeed, when considering the gold-graphene junction, due to weaker van der Waals interaction at the molecule-graphene interface, the molecule is less stretched and the DQI dip is located very close to the Fermi level. Oppositely, for the gold-gold junction, the molecular junction is more stretched which increases the angle between the two halves of the molecule, resulting in a DQI dip located further away from the Fermi level. Obviously, this stretched configuration is related to the intrinsic potentials used in the DFT calculations, which might induce some differences between the computed and measured conductance values. In addition, this specific property might also be exploited for electro-mechanical devices, as the degree of stretching of the molecule in the junction has a strong influence on the electronic conductance.

Conclusions

In this work, the conductance of *para*- and *meta*-OPE molecular wires tethered between gold-gold and gold-graphene electrodes has been measured using the STM-*I*(*s*) method. For all the molecular junctions, the *meta*-connection leads to a low conductance value, which is associated with the DQI induced dip in the transmission function which falls near the electrode Fermi level. To study the effects of electrode type on the relative position of the Fermi level and the DQI dip, amine, methyl sulfide and ethynyl anchoring groups were used to link *para*- and *meta-structured* OPEs into gold|molecule|gold and gold|molecule|graphene single molecular junctions. The electrode material has little effect on the electrical properties of the amine anchored OPEs, due to the similar electrode-molecule contacting chemistry in each case. However, for methyl sulfide and ethynyl anchored OPEs, gold-graphene electrode contacting shows a clear impact on DQI. In particular, for ethynyl anchoring OPE molecules with gold-graphene electrodes, the conductance ratio of PC/MC is greater than 400. Our study indicates that the conductance change resulting from DQI can be tuned through the connection between electrodes and anchoring groups as well as through the mechanical stress applied to the junction. The influence of electrode materials and anchoring groups on the DQI effect is clearly complex and further study is required.

Conflicts of interest

The authors declare no competing financial interest.

Acknowledgements

This work was supported by the National Natural Science Foundation of China (NSFC Grants 21503169), Suzhou Industrial Park Initiative Platform Development for Suzhou Municipal Key Lab for New Energy Technology (RR0140), Key Program Special Fund in XJTLU (KSF-E-38) and the XJTLU Research Development Fund (RDF-16-01-33 and REF-19-01-05).

Notes and references

1. X. Li, W. Ge, S. Guo, J. Bai and W. Hong, *Angew. Chem., Int. Ed.*, 2023, **62**, e202216819.
2. L. J. O'Driscoll and M. R. Bryce, *Nanoscale*, 2021, **13**, 10668-10711.
3. T. A. Su, M. Neupane, M. L. Steigerwald, L. Venkataraman and C. Nuckolls, *Nat. Rev. Mater.*, 2016, **1**, 16002.
4. H. Song, M. A. Reed and T. Lee, *Adv. Mater.*, 2011, **23**, 1583-1608.
5. L. Sun, Y. A. Diaz-Fernandez, T. A. Gschneidtner, F. Westerlund, S. Lara-Avila and K. Moth-Poulsen, *Chem. Soc. Rev.*, 2014, **43**, 7378-7411.
6. D. Z. Manrique, C. Huang, M. Baghernejad, X. Zhao, O. A. Al-Owaedi, H. Sadeghi, V. Kaliginedi, W. Hong, M. Gulcur, T. Wandlowski, M. R. Bryce and C. J. Lambert, *Nat. Commun.*, 2015, **6**, 6389.
7. C. J. Lambert, *Chem. Soc. Rev.*, 2015, **44**, 875-888.
8. T. Markussen, R. Stadler and K. S. Thygesen, *Nano Lett.*, 2010, **10**, 4260-4265.
9. C. M. Guedon, H. Valkenier, T. Markussen, K. S. Thygesen, J. C. Hummelen and S. J. van der Molen, *Nat. Nanotechnol.*, 2012, **7**, 305-309.
10. A. Borges, J. Xia, S. H. Liu, L. Venkataraman and G. C. Solomon, *Nano Lett.*, 2017, **17**, 4436-4442.
11. H. Vazquez, R. Skouta, S. Schneebeli, M. Kamenetska, R. Breslow, L. Venkataraman and M. S. Hybertsen, *Nature nanotechnology*, 2012, **7**, 663-667.
12. G. Yang, H. Wu, J. Wei, J. Zheng, Z. Chen, J. Liu, J. Shi, Y. Yang and W. Hong, *Chinese Chemical Letters*, 2018, **29**, 147-150.
13. C. R. Arroyo, S. Tarkuc, R. Frisenda, J. S. Seldenthuis, C. H. Woerde, R. Eelkema, F. C. Grozema and H. S. van der Zant, *Angew. Chem., Int. Ed. Engl.*, 2013, **52**, 3152-3155.
14. G. C. Solomon, D. Q. Andrews, R. H. Goldsmith, T. Hansen, M. R. Wasielewski, R. P. Van Duyne and M. A. Ratner, *Journal of the American Chemical Society*, 2008, **130**, 17301-17308.
15. G. C. Solomon, C. Herrmann, T. Hansen, V. Mujica and M. A. Ratner, *Nature Chemistry*, 2010, **2**, 223-228.
16. S. V. Aradhya, J. S. Meisner, M. Krikorian, S. Ahn, R. Parameswaran, M. L. Steigerwald, C. Nuckolls and L. Venkataraman, *Nano Lett.*, 2012, **12**, 1643-1647.
17. M. Kiguchi, H. Nakamura, Y. Takahashi, T. Takahashi and T. Ohto, *J. Phys. Chem. C*, 2010, **114**, 22254-22261.
18. C. J. Lambert, *Journal*, 2021, DOI: 10.1088/978-0-7503-3639-0.
19. W. Chen, H. Li, J. R. Widawsky, C. Appayee, L. Venkataraman and R. Breslow, *Journal of the American Chemical Society*, 2014, **136**, 918-920.
20. X. Liu, S. Sangtarash, D. Reber, D. Zhang, H. Sadeghi, J. Shi, Z. Y. Xiao, W. Hong, C. J. Lambert and S. X. Liu, *Angew. Chem.*, 2016, **56**, 173-176.

21. F. Jiang, D. I. Trupp, N. Algethami, H. Zheng, W. He, A. Alqorashi, C. Zhu, C. Tang, R. Li, J. Liu, H. Sadeghi, J. Shi, R. Davidson, M. Korb, A. N. Sobolev, M. Naher, S. Sangtarash, P. J. Low, W. Hong and C. J. Lambert, *Angew. Chem., Int. Ed. Engl.*, 2019, **58**, 18987-18993.
22. M. H. Garner, M. Koerstz, J. H. Jensen and G. C. Solomon, *ACS Physical Chemistry Au*, 2022, **2**, 282-288.
23. J. Bai, A. Daaoub, S. Sangtarash, X. Li, Y. Tang, Q. Zou, H. Sadeghi, S. Liu, X. Huang, Z. Tan, J. Liu, Y. Yang, J. Shi, G. Meszaros, W. Chen, C. Lambert and W. Hong, *Nat. Mater.*, 2019, **18**, 364-369.
24. Y. Li, M. Buerkle, G. Li, A. Rostamian, H. Wang, Z. Wang, D. R. Bowler, T. Miyazaki, L. Xiang, Y. Asai, G. Zhou and N. Tao, *Nat. Mater.*, 2019, **18**, 357-363.
25. B. Huang, X. Liu, Y. Yuan, Z. W. Hong, J. F. Zheng, L. Q. Pei, Y. Shao, J. F. Li, X. S. Zhou, J. Z. Chen, S. Jin and B. W. Mao, *J. Am. Chem. Soc.*, 2018, **140**, 17685-17690.
26. M. Famili, C. Jia, X. Liu, P. Wang, I. M. Grace, J. Guo, Y. Liu, Z. Feng, Y. Wang, Z. Zhao, S. Decurtins, R. Häner, Y. Huang, S.-X. Liu, C. J. Lambert and X. Duan, *Chem*, 2019, **5**, 474-484.
27. L. L. Peng, J. R. Huang, J. F. Zheng, Y. Shao, Z. J. Niu, J. F. Li, S. M. Xu and X. S. Zhou, *J. Nanosci. Nanotechnol.*, 2019, **19**, 2794-2798.
28. Y. Tsuji, T. Stuyver, S. Gunasekaran and L. Venkataraman, *J. Phys. Chem. C*, 2017, **121**, 14451-14462.
29. H. Chen, Y. Chen, H. Zhang, W. Cao, C. Fang, Y. Zhou, Z. Xiao, J. Shi, W. Chen, J. Liu and W. Hong, *Chin. Chem. Lett.*, 2022, **33**, 523-526.
30. Z.-C. Pan, J. Li, L. Chen, Y. Tang, J. Shi, J. Liu, J.-L. Liao and W. Hong, *Sci. China: Chem.*, 2019, **62**, 1245-1256.
31. D. Xiang, X. Wang, C. Jia, T. Lee and X. Guo, *Chem. Rev.*, 2016, **116**, 4318-4440.
32. A. Bellec, J. Lagoute and V. Repain, *C. R. Chim.*, 2018, **21**, 1287-1299.
33. M. Kiguchi, *Proc. Jpn. Acad., Ser. B*, 2018, **94**, 350-359.
34. E. Gorenskaia, K. L. Turner, S. Martín, P. Cea and P. J. Low, *Nanoscale*, 2021, **13**, 9055-9074.
35. I. J. Planje, R. J. Davidson, A. Vezzoli, A. Daaoub, S. Sangtarash, H. Sadeghi, S. Martin, P. Cea, C. J. Lambert, A. Beeby, S. J. Higgins and R. J. Nichols, *ACS Sens.*, 2021, **6**, 530-537.
36. T. Kim, Z.-F. Liu, C. Lee, J. B. Neaton and L. Venkataraman, *Proc. Natl. Acad. Sci.*, 2014, **111**, 10928-10932.
37. Q. Zhang, S. Tao, R. Yi, C. He, C. Zhao, W. Su, A. Smogunov, Y. J. Dappe, R. J. Nichols and L. Yang, *J. Phys. Chem. Lett.*, 2017, **8**, 5987-5992.
38. Y. Fan, S. Pitie, C. Liu, C. Zhao, C. Zhao, M. Seydou, Y. J. Dappe, R. J. Nichols and L. Yang, *The Journal of Physical Chemistry C*, 2022, **126**, 3635-3645.
39. W. Hong, D. Z. Manrique, P. Moreno-Garcia, M. Gulcur, A. Mishchenko, C. J. Lambert, M. R. Bryce and T. Wandlowski, *J. Am. Chem. Soc.*, 2012, **134**, 2292-2304.
40. K. Yoshida, I. V. Pobelov, D. Z. Manrique, T. Pope, G. Mészáros, M. Gulcur, M. R. Bryce, C. J. Lambert and T. Wandlowski, *Sci. Rep.*, 2015, **5**, 9002.
41. R. Frisenda, S. Tarkuç, E. Galán, M. L. Perrin, R. Eelkema, F. C. Grozema and H. S. J. van der Zant, *Journal*, 2015, **6**, 1558-1567.
42. Y. S. Park, J. R. Widawsky, M. Kamenetska, M. L. Steigerwald, M. S. Hybertsen, C. Nuckolls and L. Venkataraman, *J. Am. Chem. Soc.*, 2009, **131**, 10820-10821.
43. S. Tao, Q. Zhang, C. He, X. Lin, R. Xie, C. Zhao, C. Zhao, A. Smogunov, Y. J. Dappe, R. J. Nichols and L. Yang, *ACS Applied Nano Materials*, 2018, **2**, 12-18.
44. P. Pla-Vilanova, A. C. Aragonès, S. Ciampi, F. Sanz, N. Darwish and I. Diez-Perez, *Nanotechnology*, 2015, **26**, 381001.
45. L. Herrer, A. González-Orive, S. Marqués-González, S. Martín, R. J. Nichols, J. L. Serrano, P. J. Low and P. Cea, *Nanoscale*, 2019, **11**, 7976-7985.
46. W. Hong, H. Li, S.-X. Liu, Y. Fu, J. Li, V. Kaliginedi, S. Decurtins and T. Wandlowski, *J. Am. Chem. Soc.*, 2012, **134**, 19425-19431.
47. K. Sonogashira, Y. Tohda and N. Hagihara, *Tetrahedron Letters*, 1975, **16**, 4467-4470.
48. G. Casotti, G. Fusini, M. Ferreri, L. F. Pardini, C. Evangelisti, G. Angelici and A. Carpita, *Synthesis*, 2020, DOI: 10.1055/s-0039-1690852.
49. M. Guo, Z. Wei, J. Yang, Z. Xie and W. Zhang, *Catalysts*, 2020, **10**, 302.
50. F. Luo, C. Pan, L. Li, F. Chen and J. Cheng, *Chem. Commun.*, 2011, **47**, 5304-5306.
51. W. Haiss, H. van Zalinge, S. J. Higgins, D. Bethell, H. H?benreich, D. J. Schiffrin and R. J. Nichols, *Journal of the American Chemical Society*, 2003, **125**, 15294-15295.
52. B. Ren, G. Picardi and B. Pettinger, *Rev. Sci. Instrum.*, 2004, **75**, 837.
53. Q. Zhang, C. Liu, S. Tao, R. Yi, W. Su, C. Zhao, C. Zhao, Y. J. Dappe, R. J. Nichols and L. Yang, *Nanotechnology*, 2018, **29**, 325701.
54. J. P. Lewis, P. Jelínek, J. Ortega, A. A. Demkov, D. G. Trabada, B. Haycock, H. Wang, G. Adams, J. K. Tomfohr, E. Abad, H. Wang and D. A. Drabold, *Phys. Status Solidi B*, 2011, **248**, 1989-2007.
55. J. Harris, *Physical Review B*, 1985, **31**, 1770-1779.
56. M. A. Basanta, Y. J. Dappe, P. Jelínek and J. Ortega, *Computational Materials Science*, 2007, **39**, 759-766.
57. A. A. Demkov, J. Ortega, O. F. Sankey and M. P. Grumbach, *Physical Review B*, 1995, **52**, 1618-1630.
58. P. Jelínek, H. Wang, J. P. Lewis, O. F. Sankey and J. Ortega, *Physical Review B*, 2005, **71**, 235101.
59. O. F. Sankey and D. J. Niklewski, *Physical Review B*, 1989, **40**, 3979-3995.
60. S. Tao, Q. Zhang, C. He, X. Lin, R. Xie, C. Zhao, C. Zhao, A. Smogunov, Y. J. Dappe, R. J. Nichols and L. Yang, *ACS Appl. Nano Mater.*, 2018, **2**, 12-18.
61. S. Pitié, M. Seydou, Y. J. Dappe, P. Martin, F. Maurel and J. C. Lacroix, *Chemical Physics Letters*, 2022, **787**, 139273.
62. J. Tauc, R. Grigorovici and A. Vancu, *Phys. Status Solidi B*, 1966, **15**, 627-637.
63. R. H. Ramprasath, M. S. Kajamuhideen, B. Tiwari and K. Sethuraman, *J. Mater. Sci.: Mater. Electron.*, 2023, **34**, 620.
64. M. C. Scharber and N. S. Sariciftci, *Adv. Mater. Technol.*, 2021, **6**, 2000857.
65. J. C. S. Costa, R. J. S. Taveira, C. F. R. A. C. Lima, A. Mendes and L. M. N. B. F. Santos, *Opt. Mater.*, 2016, **58**, 51-60.
66. B.-G. Kim, X. Ma, C. Chen, Y. Ie, E. W. Coir, H. Hashemi, Y. Aso, P. F. Green, J. Kieffer and J. Kim, *Adv. Funct. Mater.*, 2013, **23**, 439-445.
67. F. Barrière, B. Fabre, E. Hao, Z. M. LeJeune, E. Hwang, J. C. Garno, E. E. Nesterov and M. G. H. Vicente, *Macromolecules*, 2009, **42**, 2981-2987.
68. N. El Guesmi, *ChemistrySelect*, 2023, **8**, e202203963.
69. W. Haiss, H. van Zalinge, S. J. Higgins, D. Bethell, H. H?benreich, D. J. Schiffrin and R. J. Nichols, *J. Am. Chem. Soc.*, 2003, **125**, 15294-15295.
70. R. R. Ferradás, S. Marqués-González, H. M. Osorio, J. Ferrer, P. Cea, D. C. Milan, A. Vezzoli, S. J. Higgins, R. J. Nichols, P. J. Low, V. M. García-Suárez and S. Martín, *RSC Advances*, 2016, **6**, 75111-75121.
71. Q. Lu, K. Liu, H. Zhang, Z. Du, X. Wang and F. Wang, *ACS Nano*, 2009, **3**, 3861-3868.
72. C. Huang, M. Jevric, A. Borges, S. T. Olsen, J. M. Hamill, J. T. Zheng, Y. Yang, A. Rudnev, M. Baghernejad and P. Broekmann, *Nature Communications*, **8**, 15436.
73. W. Hong, H. Li, S. X. Liu, Y. Fu, J. Li, V. Kaliginedi, S. Decurtins and T. Wandlowski, *J. Am. Chem. Soc.*, 2012, **134**, 19425-19431.
74. I. J. Olavarria-Contreras, M. L. Perrin, Z. Chen, S. Klyatskaya, M. Ruben and H. S. J. van der Zant, *J. Am. Chem. Soc.*, 2016, **138**, 8465-8469.

75. H. M. Osorio, P. Cea, L. M. Ballesteros, I. Gascón, S. Marqués-González, R. J. Nichols, F. Pérez-Murano, P. J. Low and S. Martín, *J. Mater. Chem. C*, 2014, **2**, 7348-7355.
76. L. M. Ballesteros, S. Martín, C. Momblona, S. Marqués-González, M. C. López, R. J. Nichols, P. J. Low and P. Cea, *J. Phys. Chem. C*, 2012, **116**, 9142-9150.
77. R. Miao, H. Xu, M. Skripnik, L. Cui, K. Wang, K. G. L. Pedersen, M. Leijnse, F. Pauly, K. Warnmark, E. Meyhofer, P. Reddy and H. Linke, *Nano Lett.*, 2018, **18**, 5666-5672.
78. T. A. Su, M. Neupane, M. L. Steigerwald, L. Venkataraman and C. Nuckolls, *Nature Reviews Materials*, 2016, **1**.
79. M. H. Garner, G. C. Solomon and M. Strange, *The Journal of Physical Chemistry C*, 2016, **120**, 9097-9103.
80. Q. Zhang, L. Liu, S. Tao, C. Wang, C. Zhao, C. Gonzalez, Y. J. Dappe, R. J. Nichols and L. Yang, *Nano Lett.*, 2016, **16**, 6534-6540.
81. R. A. DiStasio, G. von Helden, R. P. Steele and M. Head-Gordon, *Chem. Phys. Lett.*, 2007, **437**, 277-283.

